



Accounting for genetic effect heterogeneity in fine-mapping and improving power to detect gene-environment interactions with SharePro

Received: 27 July 2023

Accepted: 21 October 2024

Published online: 30 October 2024

 Check for updatesWenmin Zhang^{1,2} , Robert Sladek^{1,3,4}, Yue Li^{1,5}, Hamed Najafabadi^{1,3,4} & Josée Dupuis^{1,6} 


Classical gene-by-environment interaction (GxE) analysis can be used to characterize genetic effect heterogeneity but has a high multiple testing burden in the context of genome-wide association studies (GWAS). We adapt a colocalization method, SharePro, to account for effect heterogeneity in fine-mapping and identify candidates for GxE analysis with reduced multiple testing burden. SharePro demonstrates improved power for both fine-mapping and GxE analysis compared to existing methods as well as well-controlled false type I error in simulations. Using smoking status stratified GWAS summary statistics, we identify genetic effects on lung function modulated by smoking status that are not identified by existing methods. Additionally, using sex stratified GWAS summary statistics, we characterize sex differentiated genetic effects on fat distribution. In summary, we have developed an analytical framework to account for effect heterogeneity in fine-mapping and subsequently improve power for GxE analysis. The SharePro software for GxE analysis is openly available at https://github.com/zhwm/SharePro_gxe.

Genome-wide association studies (GWAS) have led to the identification of numerous genetic loci significantly associated with complex traits and diseases^{1–4}. Some genetic loci demonstrate different associations with traits and diseases in subpopulations defined by sex, environmental or lifestyle exposure status⁵. For example, the associations between variants in the *NAT2* locus and bladder cancer have different magnitudes in smokers and never smokers⁶. Characterizing such genetic effect heterogeneity can be useful in understanding biological mechanisms underlying disease heterogeneity within a population and further pinpointing modifiable risk factors for prevention and management of complex diseases⁷.

Genetic effect heterogeneity can be characterized through gene-by-environment interaction (GxE) analysis. GxE analysis is often performed by including both main effects of a genetic variant and the exposure, as well as a variant-by-exposure interaction term, one variant at a time, in a regression model. Alternatively, in the meta-analysis context, if exposure-stratified GWAS summary statistics are available, the heterogeneity test may also be performed to detect GxE⁸. However, due to a high multiple-testing burden, a large sample size is usually required to achieve sufficient power to detect GxE in the context of GWAS.

A promising approach for reducing multiple testing burdens in the context of GWAS is fine-mapping, a statistical procedure to identify

¹Quantitative Life Sciences Program, McGill University, Montréal, Canada. ²Montreal Heart Institute, Montréal, Canada. ³Department of Human Genetics, McGill University, Montréal, Canada. ⁴Dahdaleh Institute of Genomic Medicine, McGill University, Montréal, Canada. ⁵School of Computer Science, McGill University, Montréal, Canada. ⁶Department of Epidemiology, Biostatistics and Occupational Health, McGill University, Montréal, Canada.

 e-mail: wenmin.zhang@mail.mcgill.ca; josee.dupuis3@mcgill.ca

causal variants from GWAS summary statistics and linkage disequilibrium (LD) information^{9–11}. With fine-mapped variants, we can effectively reduce the number of tests required in GxE analysis. However, fine-mapping methods usually focus on the inference of causal configurations and do not assess or account for genetic effect heterogeneity, which limits their utility in GxE analysis.

In this work, we adapt SharePro, an accurate and efficient colocalization method that we recently developed¹², to account for effect heterogeneity in fine-mapping and subsequently improve power for GxE analysis. We evaluate the performance of SharePro for fine-mapping in different settings of effect heterogeneity through simulations and compare SharePro with classical methods for GxE analysis in terms of power and empirical false discovery rate (FDR). Furthermore, we examine the utility of SharePro in identifying genetic effects on lung function modulated by smoking status using smoking status stratified GWAS summary statistics. Moreover, we use SharePro to characterize genetic effect heterogeneity in fat distribution with sex stratified GWAS summary statistics.

Results

SharePro for GxE analysis

SharePro (Fig. 1) takes exposure-stratified GWAS summary statistics as input. By integrating statistical evidence from subpopulations with different exposure statuses, SharePro can effectively identify causal variants that are either shared or specific to different exposure categories, reducing the multiple testing burden in GxE analysis.

Specifically, similar to the original SharePro method for colocalization analysis¹², we use effect groups to align causal signal across exposure stratified GWAS summary statistics, thereby accounting for the uncertainty associated with identifying causal

variants due to LD. We assume that there are up to K causal signals for a phenotype y across subpopulations with different exposure categories within a locus containing G variants. For the k^{th} causal signal, we use an effect group indicator s_k to represent the causal variant and other variants that are highly correlated with it:

$$s_k \sim \text{Multinomial}\left(1, \mathbf{1}_{G \times 1} \times \frac{1}{G}\right)$$

We use c_{ke} to represent the causal status of the k^{th} effect group in the subpopulation with the e^{th} exposure category:

$$c_{ke} \sim \text{Bernoulli}(\sigma)$$

Additionally, we use β_{ke} to represent the effect size of the k^{th} effect group in the e^{th} exposure category:

$$\beta_{ke} \sim \mathcal{N}(0, \tau_\beta^{-1})$$

With the genotype matrix and the phenotype in the subpopulation with the e^{th} exposure category denoted as \mathbf{X}_e and \mathbf{y}_e , we have:

$$\mathbf{y}_e \sim \mathcal{N}\left(\mathbf{X}_e \sum_k s_k \beta_{ke} c_{ke}, \tau_y^{-1} \mathbf{I}\right)$$

Here, τ_β , τ_y and σ are hyperparameters in the model. We use similar strategies for estimating hyperparameters as in our previous work^{11,12} detailed in Supplementary Notes. Using an efficient variational inference algorithm adapted for GWAS summary statistics^{11–14}, we can obtain variant-level fine-mapping results (posterior inclusion probabilities, PIP) and identify effect groups for GxE analysis as detailed in Supplementary Notes.

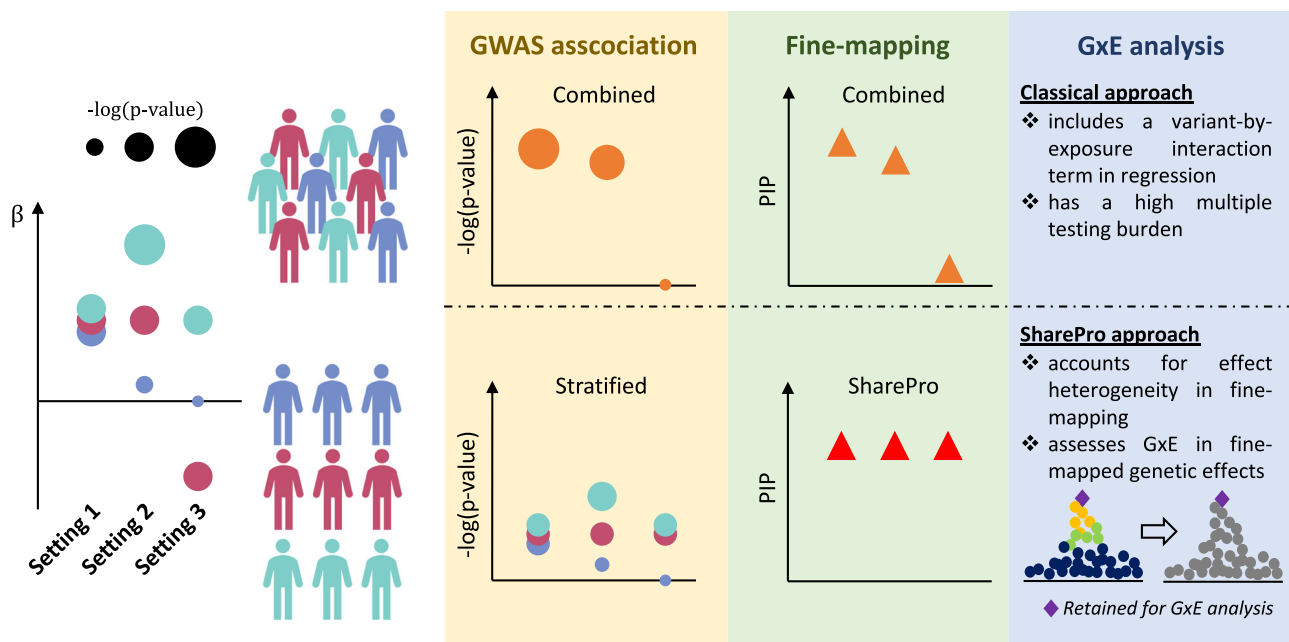


Fig. 1 | SharePro for GxE analysis. We showcase three settings of effect heterogeneity in a population with three environmental exposure statuses. In setting 1, with similar effect sizes across three exposure categories, this genetic effect can be well-characterized through combined GWAS and fine-mapping of the combined GWAS summary statistics. The stratified approaches might not be well-powered due to the relatively small sample sizes in each category. Nevertheless, with SharePro, we can fine-map this genetic effect from exposure stratified GWAS summary statistics and assess its effect heterogeneity. In setting 2, with moderate effect size discrepancy, this genetic effect may be characterized through the combined

approaches but the joint approaches will have a higher power. Classical GxE analysis can be underpowered due to a high multiple testing burden. With SharePro, we can first fine-map this genetic effect from exposure stratified GWAS summary statistics and then characterize its effect heterogeneity. With reduced multiple testing burden, we can effectively detect GxE in this setting. In setting 3, the combined approaches can no longer adequately characterize the genetic effect as two exposure categories demonstrates opposite effect sizes. With SharePro, we can accurately fine-map this genetic effect and detect its effect heterogeneity. GWAS, genome-wide association study; GxE, gene-environment interaction.

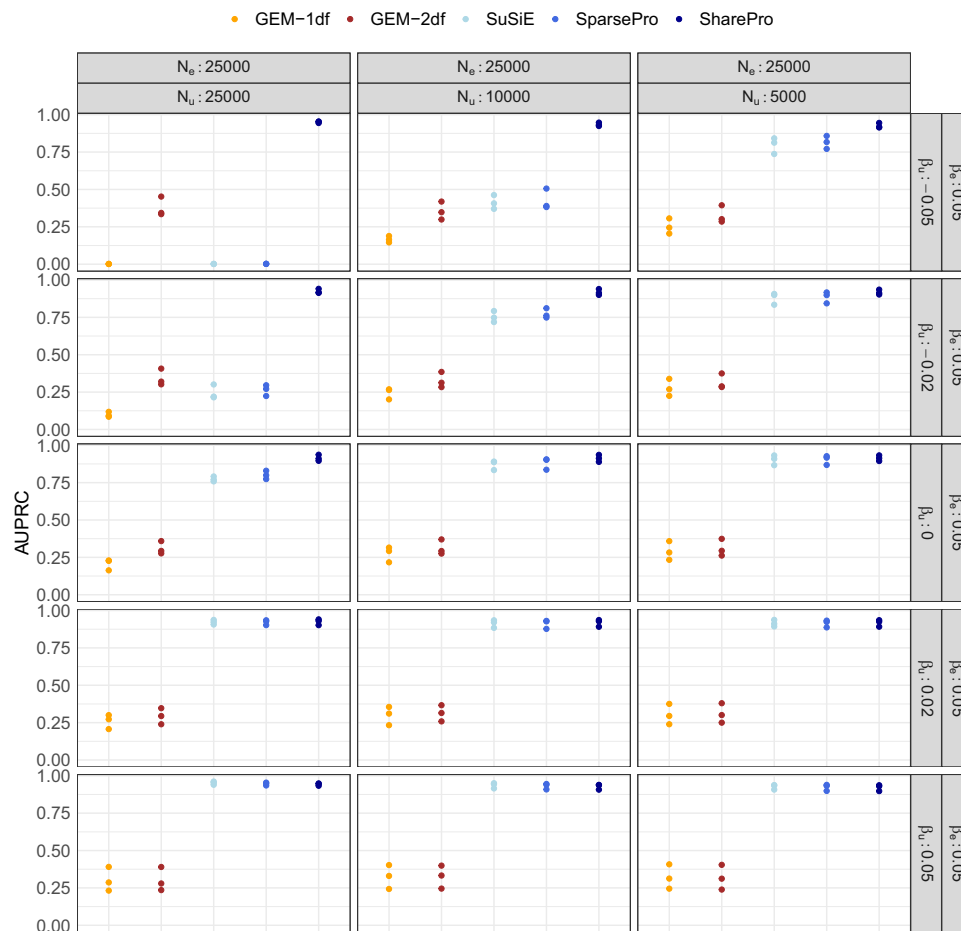


Fig. 2 | Accounting for effect heterogeneity improved power for fine-mapping.

Area under precision-recall curve (AUPRC) in simulation settings with 3 causal variants per locus ($K_C = 3$) is displayed. Rows represent different effect size discrepancies with β_e and β_u corresponding to effect size in the exposed and the unexposed category, respectively. Columns represent different sample size settings with N_e and N_u corresponding to sample size in the exposed and the

unexposed category, respectively. 1-degree of freedom (1-df) and 2-df tests were implemented in GEM. SuSiE and SparsePro were applied to the combined GWAS of the main effect (i.e. 1-df tests). Each dot indicates the AUPRC based on one of the three randomly selected loci, aggregating 50 simulation replicates under the corresponding simulation setting. Detailed statistics are provided in Supplementary Data 1.

Accounting for effect heterogeneity improved power for fine-mapping

To examine the benefits of accounting for effect heterogeneity in fine-mapping, we conducted simulation studies with varying sample sizes (N_e and N_u), effect sizes (β_e and β_u) and number of causal variants (K_C). As expected, in the presence of simulated effect heterogeneity ($\beta_e \neq \beta_u$), the 2-df association test, which accounts for effect heterogeneity, exhibited a higher AUPRC compared to the 1-df association test. SharePro fine-mapping accounted for both effect heterogeneity and LD, thereby achieving the highest AUPRC. For example, with three causal variants having an opposite effect direction and equal effect size in the exposed and the unexposed category of equal sample size ($N_e = N_u = 25,000$; $\beta_e = 0.05$; $\beta_u = -0.05$ and $K_C = 3$), the 1-df association test and the combined fine-mapping of the main effect with SparsePro and SuSiE both had an AUPRC < 0.01 , close to the AUPRC of a random predictor (Fig. 2 and Supplementary Data 1), because variant-phenotype associations in the overall population were not detectable. In contrast, the 2-df association test achieved a median AUPRC of 0.34, while SharePro fine-mapping achieved a median AUPRC of 0.95 (Fig. 2 and Supplementary Data 1).

As the opposing effect (β_u) weakened and the combined effect in the overall population ($\frac{N_e\beta_e + N_u\beta_u}{N_e + N_u}$) increased, the performance differences between methods using the joint approaches and those

employing the combined approaches attenuated. For example, with causal variants having a effect size discrepancy of 0.07 ($\beta_e = 0.05$; $\beta_u = -0.02$; $N_e = N_u = 25,000$ and $K_C = 3$), SharePro fine-mapping had a median AUPRC of 0.92 while combined fine-mapping with SuSiE and SparsePro had a median AUPRC of 0.22 and 0.27, respectively (Fig. 2 and Supplementary Data 1). Meanwhile, 2-df association test achieved a median AUPRC of 0.32 and 1-df association test only had a median AUPRC of 0.09 (Fig. 2 and Supplementary Data 1). When the effect size difference decreased to 0.05 ($\beta_e = 0.05$; $\beta_u = 0.00$), SharePro fine-mapping maintained a median AUPRC of 0.91 and SuSiE and SparsePro achieved a median AUPRC of 0.77 and 0.80 (Fig. 2 and Supplementary Data 1). Furthermore, as the effect heterogeneity decreased with reduced sample size of the unexposed category, the performance differences also attenuated. For example, with three causal variants having an opposite effect in the exposed category and the unexposed category of unequal sample sizes ($N_e = 25,000$; $N_u = 10,000$; $\beta_e = 0.05$; $\beta_u = -0.05$ and $K_C = 3$), the median AUPRC of SharePro fine-mapping was 0.93 while the median AUPRC of SuSiE and SparsePro were 0.40 and 0.39 (Fig. 2 and Supplementary Data 1). With a smaller sample size for the unexposed category ($N_u = 5000$), the median AUPRC of SharePro fine-mapping was 0.92 while the median AUPRC of SuSiE and SparsePro were 0.81 and 0.82 (Fig. 2 and Supplementary Data 1).

These trends were consistent when there was one or two causal variants (Supplementary Figs. 1–2 and Supplementary Data 1).

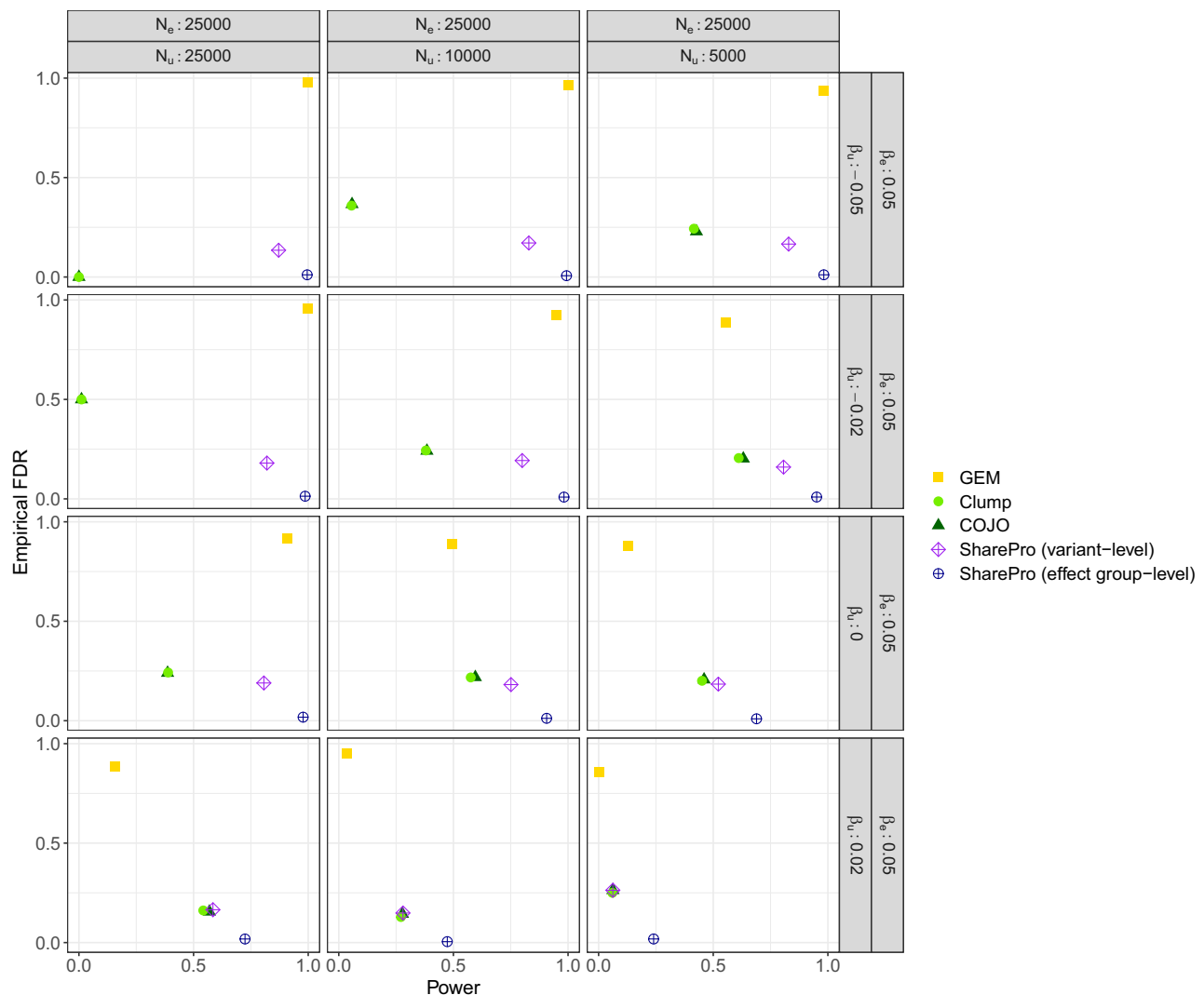


Fig. 3 | SharePro demonstrates improved power in GxE analysis. Power and empirical false discovery rate (FDR) in GxE analysis are derived with a Benjamini-Hochberg-corrected two-sided p -value cutoff of 0.01 with 3 causal variants per locus ($K_C = 3$). Rows represent different effect size discrepancies with β_e and β_u corresponding to effect size in the exposed and the unexposed category, respectively. Columns represent different sample size settings with N_e and N_u corresponding to sample size in the exposed and the unexposed category, respectively.

Variant-level GxE analysis was implemented in GEM. LD clumping (Clump) and conditional and joint (COJO) analysis were performed using the combined GWAS of the main effect. Each dot indicates the performance metrics aggregating all three randomly selected loci, each having 50 simulation replicates under the corresponding simulation setting. Detailed statistics are provided in Supplementary Data 4. Calculations of power and empirical FDR for each method are described in **Methods**.

Meanwhile, SharePro achieved the highest AUROC close to 1 across all simulation settings while the other methods could have a low AUROC in the presence of strong effect heterogeneity (e.g. $N_e = N_u = 25000$; $\beta_e = 0.05$; $\beta_u = -0.05$; Supplementary Figs 3–5 and Supplementary Data 2).

SharePro demonstrated improved power in GxE analysis

We next examined the utility of SharePro in GxE analysis and compared it to LD clumping, COJO and variant-level GxE analysis. First, without effect heterogeneity ($\beta_e = \beta_u = 0.05$), all methods provided calibrated p -values with well-controlled type I error in different simulation settings and under various significance thresholds (Supplementary Data 3). With additional 50,000 replications, the SharePro effect-group level GxE p -value maintained calibration at lower significance levels (Supplementary Fig. 6).

Importantly, SharePro consistently achieved the highest power with the lowest empirical FDR when there is effect heterogeneity. For example, when the effect size discrepancy between the exposed and the unexposed ($\beta_e - \beta_u$) was large ($\beta_e = 0.05, \beta_u = -0.05$ and $K_C = 3$), at

a p -value cutoff of 0.01, all methods achieved a similar power close to 1 (Fig. 3 and Supplementary Data 4). However, multiple testing corrected variant-level GEM p -value still had an empirical FDR of 0.98 (Fig. 3 and Supplementary Data 4). In contrast, the SharePro effect-group level GxE p -value had the lowest empirical FDR of 0.01 while the SharePro GxE p -value mapped to top variants in effect groups (SharePro variant) had an empirical FDR of 0.13 (Fig. 3 and Supplementary Data 4).

With smaller effect size discrepancy ($\beta_e - \beta_u$), SharePro maintained a high power with a low FDR, whereas other methods had decreased power. For instance, in the simulation setting with three causal variants having a effect size discrepancy of 0.03 between the exposed and the unexposed category of equal sample size ($\beta_e = 0.05$; $\beta_u = 0.0$; $N_e = N_u = 25000$ and $K_C = 3$) (Fig. 3 and Supplementary Data4), SharePro achieved a power of 0.81 with an empirical FDR of 0.19 at the variant-level and a power of 0.98 with an empirical FDR of 0.02 at the effect group-level. After multiple testing correction, GEM had a power of 0.91 with an empirical FDR of 0.91 while both lead variants identified by COJO and LD-clumping achieved a power of 0.38

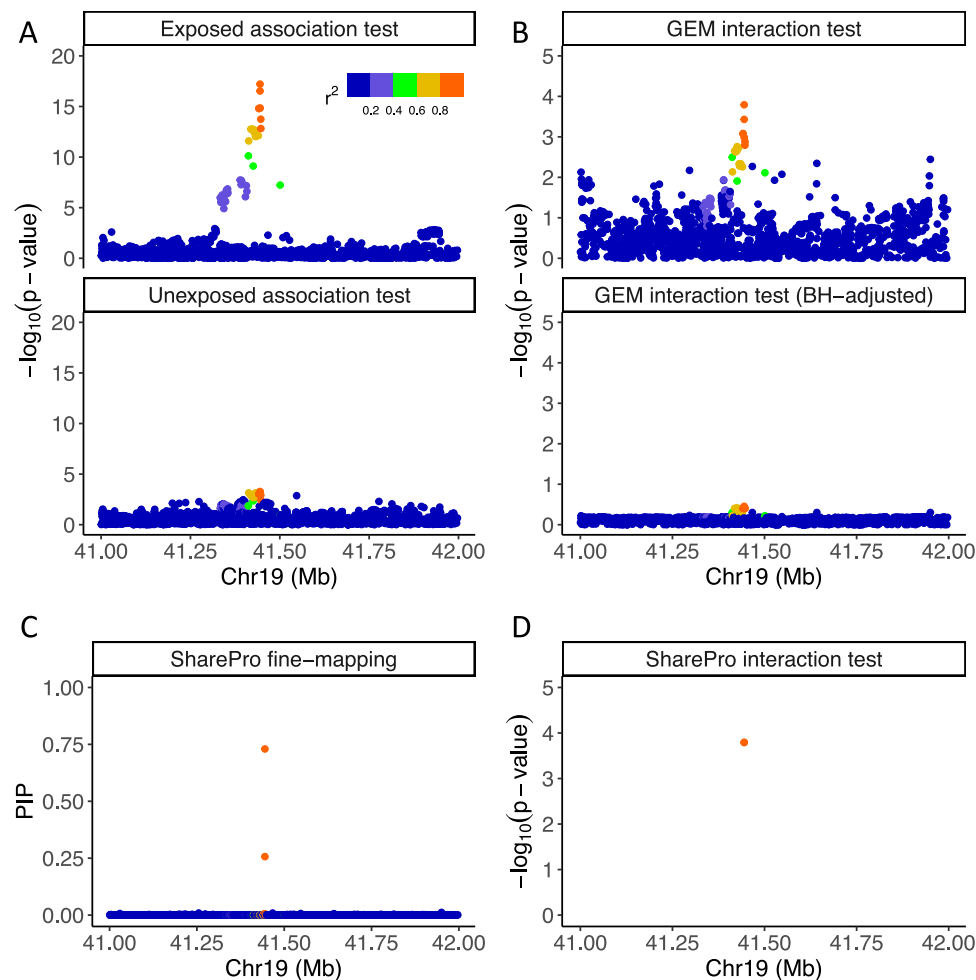


Fig. 4 | SharePro reduces multiple testing burden in GxE analysis. **A** Exposure stratified GWAS summary statistics in one simulation setting ($\beta_e = 0.05$; $\beta_u = 0.02$; $N_e = N_u = 25,000$, $K_C = 1$). Each dot represents a variant and the color indicates its squared correlation with the causal variant. **B** GEM GxE p -values and Benjamini-Hochber (BH)-adjusted GEM GxE p -values. After multiple testing corrections,

classical GxE analysis had insufficient power to detect effect heterogeneity. **C** Posterior inclusion probabilities in SharePro fine-mapping. Two variants in high LD were identified in an effect group. **D** The GxE p -value for the effect group identified in SharePro fine-mapping, represented by the top variant with the highest posterior inclusion probability in this effect group. All p -values are two-sided.

with an empirical FDR of 0.24 (Fig. 3 and Supplementary Data 4). This trend is similar with different number of causal variants (Supplementary Figs. 7–8 and Supplementary Data 4).

SharePro differs from classical GxE methods in that it uses joint fine-mapping to reduce the multiple testing burden. We illustrate the importance of this difference with a simulation example ($\beta_e = 0.05$; $\beta_u = 0.02$; $N_e = N_u = 25000$, $K_C = 1$) shown in Fig. 4. In this example, the association test in the exposed and the unexposed categories exhibited clear differences (Fig. 4A) and the GxE test in GEM accurately detected the simulated effect heterogeneity (Fig. 4B). However, the power for this test diminished after adjusting for multiple testing (Fig. 4B). In contrast, SharePro identified a candidate effect group through joint fine-mapping (Fig. 4C), thus avoiding testing on every variant, resulting in a successful GxE detection (Fig. 4D).

SharePro identified genetic effects on lung function modulated by smoking status

Based on smoking status stratified GWAS for FFR, we investigated genetic effects on lung function modulated by smoking status. Across current smokers, past smokers and never smokers, we identified 375 effect groups associated with lung function (Supplementary Data 5). The genome-wide GxE analysis only detected genome-wide significant ($p\text{-value} < 5.0 \times 10^{-8}$) effect heterogeneity mapped to the *CHRNA3* gene comparing current smokers versus past smokers, current

smokers versus never smokers, and past smokers versus never smokers (Fig. 5A). This GxSmoking interaction has been reported in literature¹⁵.

With SharePro, we also detected an effect group mapped to the *CHRNA3* gene (Fig. 5B), along with five additional effect groups with variants demonstrating different genetic effects on lung function in current smokers, past smokers and never smokers (Fig. 5C). In contrast, none of the lead variants detected by COJO and LD-clumping demonstrated significant effect heterogeneity after multiple testing correction (Supplementary Fig. 9).

Interestingly, the estimated effect sizes of these effect groups across different smoking statuses suggest potential mechanisms of GxSmoking. The effect group mapped to the *CHRNA3* gene demonstrated a large effect size in current smokers, a moderate effect size in past smokers and a minimal effect size in never smokers (Fig. 5C). The *CHRNA3* gene is known to play a significant role in nicotine dependence and smoking behaviors^{16–19}. Our results indicated that the genetic effect of *CHRNA3* on lung function may be mediated by smoking, aligning with its biological function. Moreover, the effect groups mapped to the *PRICKLE1* and the *AMZ2* genes demonstrated association with FFR in current smokers but not in previous or never smokers, while the other effect groups exhibited more complex patterns of GxSmoking interaction (Fig. 5C). *PRICKLE1* is an important regulator in the Wnt signaling pathway, which plays a crucial role in

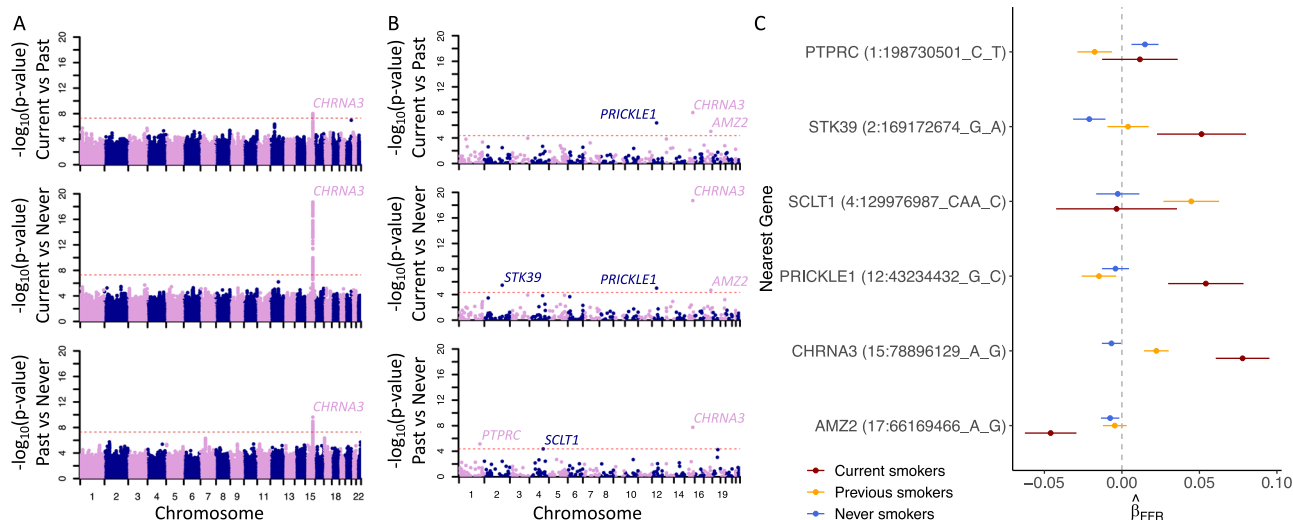


Fig. 5 | SharePro identifies genetic effects on lung function modulated by smoking status. **A** Manhattan plots demonstrating significance of genome-wide variant-level gene-by-smoking interactions (GxSmoking). The red dotted lines correspond to the genome-wide Bonferroni significance threshold. **B** Manhattan plots demonstrating significance of effect group-level GxSmoking. The red dotted lines correspond to the effect group-level Bonferroni significance threshold. Significant effect groups are labeled by their nearest genes. The unadjusted p -values are two-sided in (A) and (B). **C** Illustration of estimated effect sizes of effect groups

that exhibited significant GxSmoking effects. The smoking status stratified GWAS included 27,409 current smokers, 100,285 past smokers and 155,951 never smokers. The effect groups are annotated using their nearest genes and top variants with the highest posterior inclusion probability in each effect group. The x -axis stands for estimated effect sizes and the colors represent different smoking statuses. The error bars represent 95% confidence intervals. FFR, the ratio of the forced expiratory volume in the first one second to the forced vital capacity of the lung measured by spirometry.

inflammation and immune response, as well as development and repair of lung tissues^{20–22}. Although AMZ2 (archaelysin family metalloproteinase 2) has not been extensively studied, other human metalloproteinases have been implicated in the regulation of airway inflammation^{23,24}. Further investigations are necessary to confirm whether smoking-induced inflammation may disrupt such regulatory roles.

We repeated the analyses using inverse normal transformed FFR and obtained highly consistent results (Supplementary Fig. 10).

SharePro improved characterization of sex differentiated genetic effects on fat distribution

Based on sex stratified GWAS for WHRadjBMI, we investigated sex differentiated genetic effects on fat distribution and identified 334 effect groups associated with WHRadjBMI (Supplementary Data 6). Of these effect groups, 98 demonstrated effect group-level significance, including 47 demonstrating genome-wide significance (Supplementary Data 6).

Effect groups demonstrated significant GxSex were mapped to genes that play important roles in adipose cell biology (Supplementary Data 6). For example, *COBLL1* has been shown to play a crucial role in actin cytoskeleton remodelling during the differentiation of metabolically active and insulin-sensitive adipocytes²⁵ and has been observed to exhibit sex dimorphic expression²⁵. Recent research indicates RSPO3 can impact body fat distribution by regulating the expansion of gluteofemoral adipose tissue²⁶ while estrogen is a key regulator of adipogenesis for gluteofemoral adipocytes^{27–29}. Additionally, *KLF14* is a transcription factor that regulates gene expression in adipose tissue³⁰. Recent studies have demonstrated that *KLF14* can increase adiposity and redistribute lipid storage in female mice, but not in male mice³¹. Moreover, SharePro identified an effect group with one variant rs1534696, mapped to the *SNX10* gene, demonstrating significant GxSex in WHRadjBMI (p -value = 6.0×10^{-16} ; Supplementary Data 6). This variant has been shown to regulate diet-induced adipose expansion in female mice, but not in male mice³².

We then assessed whether these sex differentiated genetic effects could be partially attributed to known factors of sex differences,

including sex hormones and lipid metabolism. We observed that the top variants from effect groups demonstrating GxSex in WHRadjBMI tended to have sex differentiated effects on SHBG level (Spearman correlation = 0.42; p -value = 1.5×10^{-15} ; Fig. 6A). In contrast, the correlation between sex differentiated genetic effects on WHRadjBMI and sex differentiated genetic effects on bioavailable testosterone was weak (Spearman correlation = 0.05; p -value = 0.35; Fig. 6B). Since SHBG regulates both testosterone and estrogen³³, these results indicate that estrogen plays a more important role in sex differences of fat distribution. This aligns with the observation that most sex differentiated effect groups had a higher effect size in females (Supplementary Data 6) and supports the existing understanding that estrogen, rather than testosterone, promotes and maintains gluteofemoral fat distribution in females^{27–29}. Furthermore, sex differentiated genetic effects on WHRadjBMI were more correlated with sex differentiated genetic effects on TG (Spearman correlation = 0.32; p -value = 3.5×10^{-9} ; Fig. 6C) than LDL (Spearman correlation = 0.24; p -value = 1.3×10^{-5} ; Fig. 6D) and HDL (Spearman correlation = 0.16; p -value = 3.0×10^{-3} ; Fig. 6E). Notably, effect groups mapped to hormone receptor coding genes with important roles in the control of feeding behaviors^{34–36}, such as *LHCGR*, were effect group-level Bonferroni significant, which would not have been identified using the genome-wide significance threshold (Fig. 6C). After adjusting for levels of SHBG or lipids in the WHRadjBMI GWAS, the estimated GxSex interaction effects attenuated, though did not disappear (Supplementary Fig. 11), supporting that sex differentiated genetic effects on fat distribution may partially act through these molecules.

Lastly, we did not observe sex differentiated minor allele frequencies in variants included in effect groups (Fig. 6F), indicating limited impact of sex differentiated participation bias³⁷ in our study.

Discussion

In this study, we adapted SharePro, a Bayesian colocalization method¹² to propose a new framework for GxE analysis. Through extensive simulation studies, we demonstrated that accounting for effect heterogeneity can improve power for fine-mapping and by jointly fine-mapping exposure stratified GWAS summary statistics, SharePro can

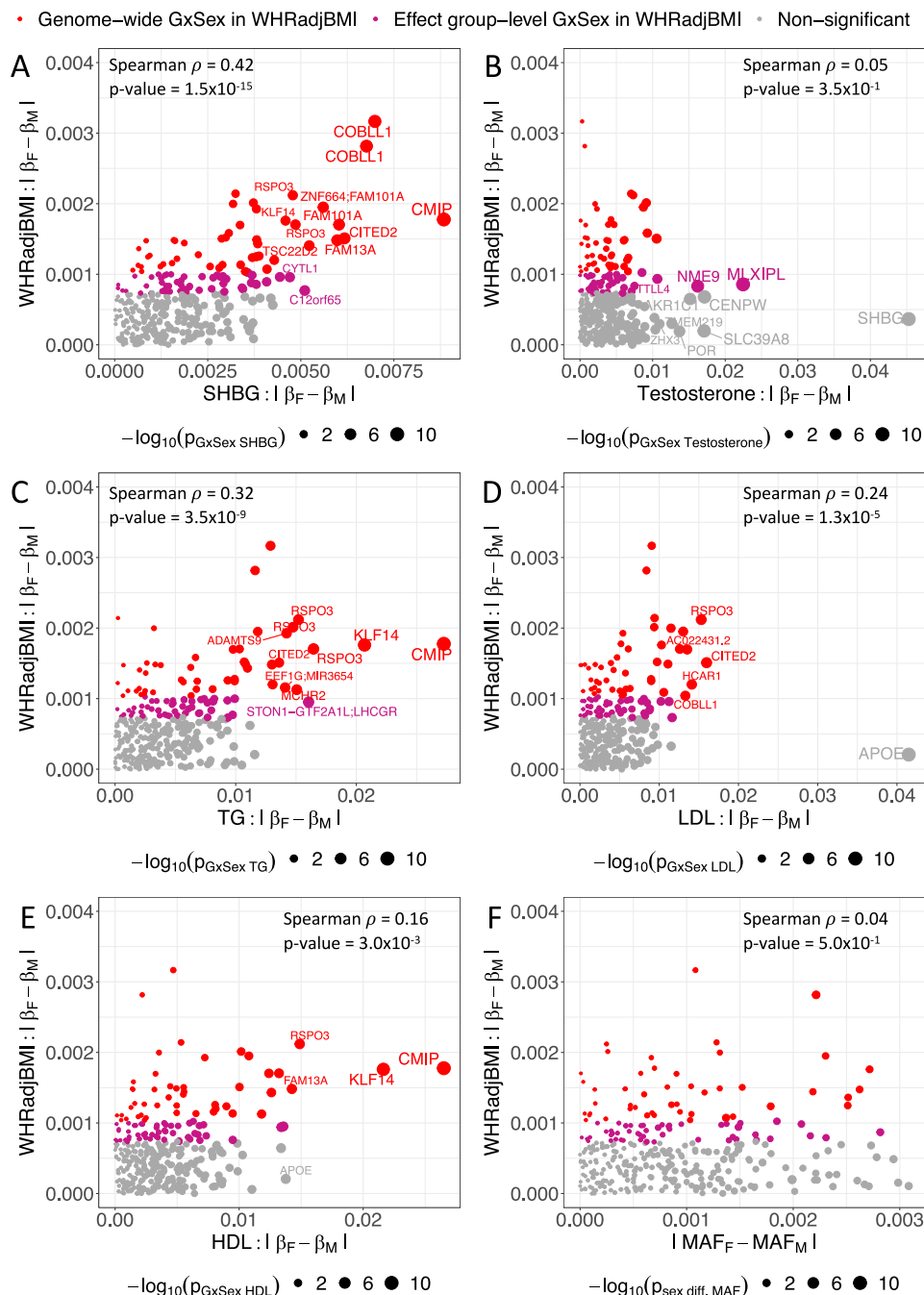


Fig. 6 | SharePro characterizes sex differentiated genetic effects on fat distribution. Effect size discrepancies in females and males for effect groups identified from sex stratified GWAS for waist-to-hip ratio adjusted for body mass index (WHRadjBMI) are plotted against (A) effect size discrepancies in females and males for sex hormone binding globulin (SHBG), (B) effect size discrepancies in females and males for bioavailable testosterone, (C) effect size discrepancies in females and males for triglycerides (TG), (D) effect size discrepancies in females and males for low-density lipoprotein (LDL) cholesterol, (E) effect size discrepancies in females

and males for high-density lipoprotein (HDL) cholesterol, and (F) minor allele frequencies (MAF) discrepancies in females and males. The size of each dot corresponds to the unadjusted two-sided p -value of the effect group. Red dots represent genome-wide significant gene-by-sex interactions (GxSex), violet dots represent effect group-level Bonferroni significant GxSex, and gray dots represent other effect groups associated with WHRadjBMI. Effect groups reaching effect group-level significance are labeled by their nearest genes.

greatly reduce multiple testing burden in GxE analysis and achieve improved power with well-controlled type I error.

The idea of accounting for effect heterogeneity to improve power for fine-mapping is closely connected with the work by Kraft et al.³⁸ on exploiting GxE to detect genetic associations. As illustrated in Fig. 1, the joint approach offers advantages over the combined approach in scenarios involving effect heterogeneity, while also outperforming the stratified approach.

Furthermore, this work represents a first attempt to bridge fine-mapping and GxE analysis. In comparison to methods and study designs that screen variants based on certain assumptions to mitigate the multiple testing burden in GxE analysis^{5,7}, the joint fine-mapping approach in SharePro offers the advantage of not involving additional assumptions. As a result, SharePro demonstrated robust performance across different heterogeneity settings. The SharePro approach is effective as long as the exposure stratified GWAS summary statistics

are well-powered to be fine-mapped. Compared to pooling-based methods such as polygenic risk score (PRS)-based GxE analysis³⁹, GxE detected by SharePro has better interpretability, as PRS can involve variants associated with multiple complicated pathways.

With improved power for GxE analysis, SharePro successfully identified additional genetic effects on lung function modulated by smoking status, which were not captured by the classical heterogeneity test. In comparison to the well-characterized *CHRNA3* gene, the biological roles of the other genes in relation to smoking are understudied, highlighting the need for further investigations, in particular, regarding their physiological roles in cellular response to smoking.

Using SharePro, we also characterized sex differentiated genetic effects on fat distribution as measured by WHRadjBMI. Our findings suggest that SHBG or other sex hormones regulated by SHBG, such as estradiol, may play a more important role than testosterone in shaping the sex differences in fat distribution. Moreover, we observed a correlation between sex differences in fat distribution and sex differences in lipid metabolism, particularly in relation to TG levels. These results underscore the ability of SharePro to detect biologically plausible GxE and identify potential candidates for subsequent functional follow-up studies.

However, there are also important limitations in our study. First, the genetic effect heterogeneity detected by SharePro should be carefully interpreted based on the study design of the exposure stratified GWAS. For example, the sex differentiated genetic effects on fat distribution we identified may not reflect the actual biological differences between females and males. Instead, these differences could originate from other lifestyle factors demonstrating sex differences, such as dietary habits and physical activities^{40–42}. Second, SharePro takes exposure stratified GWAS summary statistics and LD information as input and the mismatch between the LD reference panel and the true LD structure underlying samples included in GWAS can lead to convergence issue of the algorithm. We suggest using GWAS summary statistics with paired in-sample LD information to mitigate this issue. Third, in the SharePro model, we assume the LD structures are similar across different exposure categories so that it becomes reasonable to assume the variant representations of effect groups can be shared. This assumption is unlikely to be valid when populations with different genetic ancestries are included. Further adaptations are needed for GxE analysis in such scenarios, given the increasing interests in identifying potential GxE in diverse populations.

In summary, we have presented SharePro to account for effect heterogeneity in fine-mapping and improve the power of GxE analysis. We envision this new analytical framework will have important utility in characterizing genetic effects heterogeneity in complex traits and diseases and identifying modifiable risk factors for prevention and management of complex diseases.

Methods

Ethical approval

This study was approved by the UK Biobank Access Committee. The UK Biobank was approved by the North West Multi-center Research Ethics Committee.

Simulation study design

We conducted simulation studies to examine the benefits of accounting for effect heterogeneity in fine-mapping and assess the utility of SharePro in GxE analysis. We randomly sampled three 1-Mb regions from the genome and extracted genotypes for $N_e \in \{25000\}$ and $N_u \in \{25000, 10000, 5000\}$ non-overlapping individuals from a total of 353,570 UK Biobank unrelated European ancestry participants¹ to simulate the phenotype in the exposed category and the unexposed category, respectively. The UK Biobank participants were genotyped

using the Applied Biosystems™ UK BiLEVE Axiom™ Array or UK Biobank Axiom™ Array¹. The genotypes were imputed based on the Haplotype Reference Consortium reference panel⁴³. We retained variants that had a minor allele frequency > 0.01 , a missing rate < 0.01 , and an imputation information score > 0.3 . For each locus, we randomly sampled $K_C \in \{1, 2, 3\}$ causal variants with effect size $\beta_e \in \{0.05\}$ in the exposed category and effect size $\beta_u \in \{-0.05, -0.02, 0, 0.02, 0.05\}$ in the unexposed category. The phenotype was generated as $y_{i,e} = \sum_g x_{i,g,e} \beta_e + \epsilon_{i,e}$ for the i^{th} individual in the exposed category and $y_{j,u} = \sum_g x_{j,g,u} \beta_u + \epsilon_{j,u}$ for the j^{th} individual in the unexposed category, where $x_{i,g,e}$ and $x_{j,g,u}$ are the standardized genotype of the g^{th} designated causal variant of these individuals. The residual errors are normally distributed with $\epsilon_{i,e} \sim \mathcal{N}(0, 1 - K_C \beta_e^2)$ and $\epsilon_{j,u} \sim \mathcal{N}(0, 1 - K_C \beta_u^2)$.

We used the simulation setting of $\beta_e = \beta_u = 0.05$ (no effect heterogeneity) to assess the calibration of different methods at p -value cutoffs of 0.1, 0.01 and 0.001. The simulation process was repeated 50 times for each setting in each locus. We conducted additional 50,000 replications in each setting to assess the calibration of SharePro at lower significance levels.

Association test and fine-mapping in simulation studies

We first used PLINK⁴⁴ to perform a GWAS separately in the exposed category and the unexposed category and obtained exposure stratified GWAS summary statistics for each simulated phenotype. We also performed regression analyses with individual-level genotype and exposure status to obtain results for the 1-df association test, the 2-df association test and the GxE test. These tests were implemented in GEM⁴⁵. Specifically, the 1-df association test assesses the marginal variant-phenotype associations, combining data from all exposure categories, with the null hypothesis that the tested variant has no main effect. The GxE test assesses whether variant-phenotype associations differ across exposure categories, with the null hypothesis that the tested variant has no interaction effect with the exposure. The 2-df association test jointly assesses variant-phenotype associations and association magnitude differences across exposure categories, with the null hypothesis that the tested variant does not have main effect or interaction effect³⁸.

For fine-mapping, we first applied SuSiE and SparsePro, two state-of-the-art fine-mapping methods with the 1-df association test GWAS summary statistics and in-sample LD. Then, we applied SharePro with the exposure stratified GWAS summary statistics and in-sample LD. We compared the area under the precision-recall curve (AUPRC) and area under the receiver operating characteristic curve (AUROC) in identifying causal variants using SuSiE fine-mapping PIP, SparsePro fine-mapping PIP, SharePro fine-mapping PIP, the negative logarithm of 1-df association test p -values and the negative logarithm of 2-df association test p -values as predictors, respectively. We focused on the AUPRC metric because the proportion of true causal variants was small. The baseline AUPRC of a random predictor is the proportion of true causal variants.

GxE analysis in simulation studies

Then, we performed GxE analysis using the simulated data. Variant-level GxE p -values were obtained using GEM. For SharePro, we identified effect groups as candidates for GxE analysis, where the significance of GxE effect was determined based on the top variants with the highest PIP in each effect group (Supplementary Notes). Since variants with GxE effects may be enriched in genome-wide significant loci, we compared SharePro to performing GxE analysis only on lead variants identified in conditional and joint (COJO) analysis or LD clumping of the 1-df association test GWAS summary statistics. LD clumping was conducted using PLINK⁴⁴ with $-p1$ 5e-8, $-clump$ -kb 3000, and $-clump$ -r2 0.01. COJO analysis was conducted using GCTA-COJO⁴⁶ using the default settings.

For each method, we obtained the Benjamini-Hochberg-corrected p -values, accounting for the respective number of tests. The power and empirical FDR of GEM, COJO, and LD clumping were calculated as $\{\text{Number of variants with true GxE effects and a GxE test corrected } p\text{-value} < 0.01\} / \{\text{Number of variants with true GxE effects}\}$ and $\{\text{Number of variants without true GxE effects but having a GxE test corrected } p\text{-value} < 0.01\} / \{\text{Number of variants with a GxE test corrected } p\text{-value} < 0.01\}$, respectively. The power and empirical FDR of SharePro at the effect group level were calculated as $\{\text{Number of effect groups with a GxE test corrected } p\text{-value} < 0.01 \text{ while containing variants with true GxE effects}\} / \{\text{Number of effect groups containing variants with true GxE effects}\}$ and $\{\text{Number of effect groups with a GxE test corrected } p\text{-value} < 0.01 \text{ while not containing any variants with true GxE effects}\} / \{\text{Number of effect groups with a GxE test corrected } p\text{-value} < 0.01\}$, respectively. Although the effect group-level test is the proposed approach for GxE analysis, to ensure a fair comparison with the other methods, we also derived the power and empirical FDR of SharePro at the variant level as $\{\text{Number of top variants with true GxE effects and a GxE test corrected } p\text{-value} < 0.01\} / \{\text{Number of top variants with true GxE effects}\}$ and $\{\text{Number of top variants without true GxE effects but having a GxE test corrected } p\text{-value} < 0.01\} / \{\text{Number of top variants with a GxE test corrected } p\text{-value} < 0.01\}$, respectively.

Gene-by-smoking interaction effects on lung function

Smoking is one of the most common risk factors for chronic obstructive pulmonary disease and has a significant impact on lung function⁴⁷. We investigated genetic effects on lung function that may be modulated by smoking status. Specifically, we focused on analyzing the ratio of the forced expiratory volume in the first one second to the forced vital capacity of the lung measured by spirometry (FFR), a widely used biomarker for lung function.

For FFR, we first performed self-reported smoking status stratified GWAS as well as combined GWAS adjusted for smoking status based on unrelated individuals of European ancestry in the UK Biobank¹, including 27,409 current smokers, 100,285 past smokers and 155,951 never smokers. FFR measurement was adjusted for age, age-squared, sex, genotyping array, recruitment center, and the first 20 genetic principal components in the stratified analysis.

Then, we applied SharePro to these smoking status stratified GWAS summary statistic with the UK Biobank European ancestry LD matrix calculated by Weissbrod et al.⁴⁸ and identified effect groups for GxE analysis. Effect groups with a gene-by-smoking interactions (GxSmoking) $p\text{-value} < \frac{0.05}{\text{number of comparisons}}$ were considered effect group-level Bonferroni significant. We annotated each effect group to the nearest protein coding gene based on UCSC genome annotations⁴⁹. Additionally, with smoking status-adjusted combined GWAS, we performed LD clumping using PLINK with $-p1$ 5e-8, $-clump\text{-kb}$ 3000, and $-clump\text{-r2}$ 0.01 and COJO analysis using GCTA-COJO with default settings. Subsequently, lead variants identified in LD clumping and COJO analysis were included in GxE analysis. Variants with a GxSmoking $p\text{-value} < \frac{0.05}{\text{number of comparisons}}$ were considered Bonferroni significant for each method.

Since it has been shown that transformation of data may lead to false positive findings in similar analyzes¹⁵, we focused on analyzing raw values of FFR but performed sensitivity analyzes using inverse normal transformed FFR.

Gene-by-sex interaction effects on fat distribution

Fat distribution has important implications for health and is associated with metabolic and cardiovascular diseases^{50–52}. We investigated sex-differentiated genetic effects on body fat distribution, measured by waist-to-hip ratio adjusted for body mass index (WHRadjBMI). We performed sex stratified GWAS for WHRadjBMI in individuals of European ancestry in the UK Biobank¹, including 189,830 females and 162,508 males. We regressed out the effects of body mass index, age,

age-squared, sex, genotyping array, recruitment center, and the first 20 genetic principal components on raw waist-to-hip ratio measurements. We applied SharePro to the sex stratified GWAS summary statistics with the UK Biobank European ancestry LD matrix calculated by Weissbrod et al.⁴⁸. Effect groups with a gene-by-sex interactions (GxSex) $p\text{-value}$ smaller than $\frac{0.05}{\text{number of comparisons}}$ were considered effect group-level Bonferroni significant. We annotated each effect group to the nearest protein coding gene based on UCSC genome annotations⁴⁹.

Next, we investigated whether GxSex in WHRadjBMI may be explained by GxSex in sex hormones and lipid metabolism. We obtained sex stratified GWAS summary statistics for bioavailable testosterone and sex hormone binding globulin (SHBG) for UK Biobank European ancestry from Ruth et al.⁵³. Additionally, we performed sex stratified GWAS using European ancestry individuals in the UK Biobank for triglycerides (TG), low density lipoprotein cholesterol (LDL) and high density lipoprotein cholesterol (HDL). For effect groups that demonstrated significant GxSex, we further investigated whether the GxSex interaction effects would attenuate after adjusting for the levels of SHBG or lipids in the GWAS for WHRadjBMI.

Moreover, we examined whether variants in effect groups exhibited different MAF in females and males, which could indicate sex differentiated participation bias³⁷. We obtained p -values for sex differentiated MAF from z -scores:

$$z_{MAF} = \frac{p_F - p_M}{\sqrt{p(1-p)\left(\frac{1}{2n_F} + \frac{1}{2n_M}\right)}} \quad (1)$$

where p_F and p_M are MAF in females and males, n_F and n_M correspond to female and male sample sizes, and p is the overall MAF.

Reporting summary

Further information on research design is available in the Nature Portfolio Reporting Summary linked to this article.

Data availability

Raw individual-level phenotype and genotype data from the UK Biobank are available under restricted access for confidentiality reasons. Access can be obtained upon successful application at <https://www.ukbiobank.ac.uk>. The full GWAS summary statistics for FFR and WHRadjBMI, along with SharePro, LD clumping, and COJO results generated in this study are provided in a figshare repository, accessible via <https://doi.org/10.6084/m9.figshare.25959295.v2>. The simulated data generated in this study can be reproduced using code available at https://github.com/zhwm/SharePro_gxe_analysis.

Code availability

The SharePro software⁵⁴ for GxE analysis is openly available at https://github.com/zhwm/SharePro_gxe. The analysis conducted in this study is available at https://github.com/zhwm/SharePro_gxe_analysis. GEM was obtained from GitHub at <https://github.com/large-scale-gxe-methods/GEM> and PLINK was obtained from <https://www.cog-genomics.org/plink/>. COJO was obtained from <https://yanglab.westlake.edu.cn/software/gcta>.

References

1. Bycroft, C. et al. The UK biobank resource with deep phenotyping and genomic data. *Nature* **562**, 203–209 (2018).
2. Canela-Xandri, O., Rawlik, K. & Tenesa, A. An atlas of genetic associations in UK biobank. *Nat. Genet.* **50**, 1593–1599 (2018).
3. Loh, P.-R., Kichaev, G., Gazal, S., Schoech, A. P. & Price, A. L. Mixed-model association for biobank-scale datasets. *Nat. Genet.* **50**, 906–908 (2018).

4. Visscher, P. M. et al. 10 years of GWAS discovery: biology, function, and translation. *Am. J. Hum. Genet.* **101**, 5–22 (2017).
5. Ritz, B. R. et al. Lessons learned from past gene-environment interaction successes. *Am. J. Epidemiol.* **186**, 778–786 (2017).
6. Garcia-Closas, M. et al. Nat2 slow acetylation, gstm1 null genotype, and risk of bladder cancer: results from the spanish bladder cancer study and meta-analyses. *Lancet* **366**, 649–659 (2005).
7. Thomas, D. Gene-environment-wide association studies: emerging approaches. *Nat. Rev. Genet.* **11**, 259–272 (2010).
8. Magi, R., Lindgren, C. M. & Morris, A. P. Meta-analysis of sex-specific genome-wide association studies. *Genet. Epidemiol.* **34**, 846–853 (2010).
9. Benner, C. et al. Finemap: efficient variable selection using summary data from genome-wide association studies. *Bioinformatics* **32**, 1493–1501 (2016).
10. Wang, G., Sarkar, A., Carbonetto, P. & Stephens, M. A simple new approach to variable selection in regression, with application to genetic fine mapping. *J. R. Stat. Soc. Ser. B: Stat. Methodol.* **82**, 1273–1300 (2020).
11. Zhang, W., Najafabadi, H. & Li, Y. Sparsepro: An efficient fine-mapping method integrating summary statistics and functional annotations. *PLoS Genet.* **19**, e1011104 (2023).
12. Zhang, W. et al. Sharepro: an accurate and efficient genetic colocalization method accounting for multiple causal signals. *Bioinformatics* **40**, btac295 (2024).
13. Blei, D. M., Kucukelbir, A. & McAuliffe, J. D. Variational inference: a review for statisticians. *J. Am. Stat. Assoc.* **112**, 859–877 (2017).
14. Titsias, M. & Lazaro-Gredilla, M. Spike and slab variational inference for multi-task and multiple kernel learning. *Adv. Neural Inf. Process. Syst.* **24**, 2339–2347 (2011).
15. Wang, H. et al. Genotype-by-environment interactions inferred from genetic effects on phenotypic variability in the uk biobank. *Sci. Adv.* **5**, eaaw3538 (2019).
16. Ware, J. J., van den Bree, M. & Munafò, M. R. From men to mice: Chrna5/chrna3, smoking behavior and disease. *Nicotine Tob. Res.* **14**, 1291–1299 (2012).
17. Kaur-Knudsen, D., Nordestgaard, B. G. & Bojesen, S. E. Chrna3 genotype, nicotine dependence, lung function and disease in the general population. *Eur. Respiratory J.* **40**, 1538–1544 (2012).
18. Liu, M. et al. Association studies of up to 1.2 million individuals yield new insights into the genetic etiology of tobacco and alcohol use. *Nat. Genet.* **51**, 237–244 (2019).
19. Xu, K. et al. Genome-wide association study of smoking trajectory and meta-analysis of smoking status in 842,000 individuals. *Nat. Commun.* **11**, 5302 (2020).
20. Tree, D. R. et al. Prickle mediates feedback amplification to generate asymmetric planar cell polarity signaling. *Cell* **109**, 371–381 (2002).
21. Zallen, J. A. Planar polarity and tissue morphogenesis. *Cell* **129**, 1051–1063 (2007).
22. Aros, C. J., Pantoja, C. J. & Gomperts, B. N. Wnt signaling in lung development, regeneration, and disease progression. *Commun. Biol.* **4**, 601 (2021).
23. Paulissen, G. et al. Role of adam and adamts metalloproteinases in airway diseases. *Respiratory Res.* **10**, 1–12 (2009).
24. Drey Mueller, D., Uhlig, S. & Ludwig, A. Adam-family metalloproteinases in lung inflammation: potential therapeutic targets. *Am. J. Physiol. -Lung Cell. Mol. Physiol.* **308**, L325–L343 (2015).
25. Glunk, V. et al. A non-coding variant linked to metabolic obesity with normal weight affects actin remodelling in subcutaneous adipocytes. *Nat. Metab.* **5**, 861–879 (2023).
26. Loh, N. Y. et al. Rspo3 impacts body fat distribution and regulates adipose cell biology in vitro. *Nat. Commun.* **11**, 2797 (2020).
27. Cox-York, K. A., Erickson, C. B., Pereira, R. I., Bessesen, D. H. & Van Pelt, R. E. Region-specific effects of oestradiol on adipose-derived stem cell differentiation in post-menopausal women. *J. Cell. Mol. Med.* **21**, 677–684 (2017).
28. Frank, A. P., de Souza Santos, R., Palmer, B. F. & Clegg, D. J. Determinants of body fat distribution in humans may provide insight about obesity-related health risks. *J. Lipid Res.* **60**, 1710–1719 (2019).
29. Brown, L. & Clegg, D. Central effects of estradiol in the regulation of food intake, body weight, and adiposity. *J. Steroid Biochem. Mol. Biol.* **122**, 65–73 (2010).
30. Small, K. S. et al. Regulatory variants at klfl4 influence type 2 diabetes risk via a female-specific effect on adipocyte size and body composition. *Nat. Genet.* **50**, 572–580 (2018).
31. Yang, Q. et al. Adipocyte-specific modulation of klfl4 expression in mice leads to sex-dependent impacts on adiposity and lipid metabolism. *Diabetes* **71**, 677–693 (2022).
32. Hansen, G. T. et al. Genetics of sexually dimorphic adipose distribution in humans. *Nat. Genet.* **55**, 461–470 (2023).
33. Selby, C. Sex hormone binding globulin: origin, function and clinical significance. *Ann. Clin. Biochem.* **27**, 532–541 (1990).
34. Qu, D. et al. A role for melanin-concentrating hormone in the central regulation of feeding behaviour. *Nature* **380**, 243–247 (1996).
35. Al-Massadi, O. et al. Multifaceted actions of melanin-concentrating hormone on mammalian energy homeostasis. *Nat. Rev. Endocrinol.* **17**, 745–755 (2021).
36. Kim, K. et al. Dairy food intake is associated with reproductive hormones and sporadic anovulation among healthy premenopausal women. *J. Nutr.* **147**, 218–226 (2017).
37. Pirastu, N. et al. Genetic analyses identify widespread sex-differential participation bias. *Nat. Genet.* **53**, 663–671 (2021).
38. Kraft, P., Yen, Y.-C., Stram, D. O., Morrison, J. & Gauderman, W. J. Exploiting gene-environment interaction to detect genetic associations. *Hum. Heredity* **63**, 111–119 (2007).
39. Aschard, H. et al. Evidence for large-scale gene-by-smoking interaction effects on pulmonary function. *Int. J. Epidemiol.* **46**, 894–904 (2017).
40. Eilat-Adar, S. et al. Dietary patterns and their association with cardiovascular risk factors in a population undergoing lifestyle changes: the strong heart study. *Nutr., Metab. Cardiovascular Dis.* **23**, 528–535 (2013).
41. Ambrosini, G. L. et al. Dietary patterns and markers for the metabolic syndrome in australian adolescents. *Nutr., Metab. Cardiovascular Dis.* **20**, 274–283 (2010).
42. Panagiotakos, D. B., Pitsavos, C., Skoumas, Y. & Stefanadis, C. The association between food patterns and the metabolic syndrome using principal components analysis: The attica study. *J. Am. Dietetic Assoc.* **107**, 979–987 (2007).
43. A reference panel of 64,976 haplotypes for genotype imputation. *Nat. Genet.* **48**, 1279–1283 (2016).
44. Purcell, S. et al. Plink: a tool set for whole-genome association and population-based linkage analyses. *Am. J. Hum. Genet.* **81**, 559–575 (2007).
45. Westerman, K. E. et al. Gem: scalable and flexible gene-environment interaction analysis in millions of samples. *Bioinformatics* **37**, 3514–3520 (2021).
46. Yang, J. et al. Conditional and joint multiple-snp analysis of gwas summary statistics identifies additional variants influencing complex traits. *Nat. Genet.* **44**, 369–375 (2012).
47. Organization, W. H. et al. *Tobacco Or Health: A Global Status Report* (World Health Organization, 1997).
48. Weissbrod, O. et al. Functionally informed fine-mapping and polygenic localization of complex trait heritability. *Nat. Genet.* **52**, 1355–1363 (2020).
49. Karolchik, D. et al. The UCSC genome browser database. *Nucleic Acids Res.* **31**, 51–54 (2003).

50. Després, J.-P. Body fat distribution and risk of cardiovascular disease: an update. *Circulation* **126**, 1301–1313 (2012).
51. Valenzuela, P. L. et al. Obesity and the risk of cardiometabolic diseases. *Nat. Rev. Cardiol.* **20**, 475–494 (2023).
52. Neeland, I. J. et al. Body fat distribution and incident cardiovascular disease in obese adults. *J. Am. Coll. Cardiol.* **65**, 2150–2151 (2015).
53. Ruth, K. S. et al. Using human genetics to understand the disease impacts of testosterone in men and women. *Nat. Med.* **26**, 252–258 (2020).
54. Zhang, W. et al. Accounting for genetic effect heterogeneity in fine-mapping and improving power to detect gene-environment interactions with SharePro <https://doi.org/10.6084/m9.figshare.25959295.v2> (2024).

Acknowledgements

W.Z. has been supported by a doctoral training fellowship from the FRQNT (319188) and the Healthy Brains, Healthy Lives Program, funded by the Canada First Research Excellence Fund (CFREF), Quebec's Ministère de l'Économie et de l'Innovation (MEI), and the Fonds de recherche du Québec (FRQS, FRQSC and FRQNT). Y.L. is supported by Natural Sciences and Engineering Research Council (NSERC) Discovery Grant (RGPIN-2019-0621), Fonds de recherche Nature et Technologies (FRQNT) New Career (NC-268592), and Canada First Research Excellence Fund Healthy Brains for Healthy Life (HBHL) initiative New Investigator start-up award (G249591). H.S.N holds a Canada Research Chair funded by the Canadian Institutes of Health Research and has been supported by NSERC Discovery Grant (RGPIN-2018-05962). This research used the NeuroHub infrastructure and was undertaken thanks in part to funding from the Canada First Research Excellence Fund, awarded through the Healthy Brains, Healthy Lives initiative at McGill University. This research was enabled in part by support provided by Calcul Québec and the Digital Research Alliance of Canada. This research has been conducted using the UK Biobank Resource under Application Number 45551.

Author contributions

Conceptualization: W.Z.; Data curation: W.Z.; Formal analysis: W.Z.; Funding Acquisition: W.Z., Y.L., H.S.N and J.D.; Investigation: W.Z.; Methodology: W.Z.; Project Administration: R.S., H.S.N and J.D.; Resources: Y.L., H.S.N and J.D.; Software: W.Z.; Supervision: Y.L., R.S., H.S.N and J.D.; Validation: W.Z., R.S., Y.L., H.S.N and J.D.; Visualization: W.Z.; Writing - Original Draft Preparation: W.Z.; Writing - Review & Editing: W.Z., R.S., Y.L., H.S.N and J.D.

Competing interests

The authors declare no competing interests.

Additional information

Supplementary information The online version contains supplementary material available at <https://doi.org/10.1038/s41467-024-53818-w>.

Correspondence and requests for materials should be addressed to Wenmin Zhang or Josée Dupuis.

Peer review information *Nature Communications* thanks Brandon Coombes, Huanwei Wang, and the other, anonymous, reviewer(s) for their contribution to the peer review of this work. A peer review file is available.

Reprints and permissions information is available at <http://www.nature.com/reprints>

Publisher's note Springer Nature remains neutral with regard to jurisdictional claims in published maps and institutional affiliations.

Open Access This article is licensed under a Creative Commons Attribution-NonCommercial-NoDerivatives 4.0 International License, which permits any non-commercial use, sharing, distribution and reproduction in any medium or format, as long as you give appropriate credit to the original author(s) and the source, provide a link to the Creative Commons licence, and indicate if you modified the licensed material. You do not have permission under this licence to share adapted material derived from this article or parts of it. The images or other third party material in this article are included in the article's Creative Commons licence, unless indicated otherwise in a credit line to the material. If material is not included in the article's Creative Commons licence and your intended use is not permitted by statutory regulation or exceeds the permitted use, you will need to obtain permission directly from the copyright holder. To view a copy of this licence, visit <http://creativecommons.org/licenses/by-nc-nd/4.0/>.

© The Author(s) 2024